



# Control of Laminar Separation Bubble using Vortex Generators

N. K. Singh

*Department of Mechanical Engineering, National Institute of Technology, Kurukshetra, Haryana, 136119, India*

†Corresponding Author Email: [nksinghfme@nitkk.ac.in](mailto:nksinghfme@nitkk.ac.in)

(Received May 5, 2018; accepted October 12, 2018)

## ABSTRACT

In this paper, the performance of sub boundary layer vortex generators and conventional vortex generators in controlling the separation bubble has been compared and the resultant highly three-dimensional flow has been studied. Two pairs of vortex generators mounted symmetrically along the spanwise direction are placed upstream of separation point to produce counter-rotating vortices. Effect of these three-dimensional vortex generators on the separation bubble and the flow downstream has been examined. The simulations show that the length of the separation bubble is reduced by sixty two per cent due to the deployment of vortex generators of height  $0.33 \delta$  while the original separation bubble is completely eliminated by the vortex generators of height  $0.66 \delta$ . However the presence of larger height vortex generators by itself causes a small mean separation bubble downstream. The flow downstream of vortex generators is highly three-dimensional and zones of recirculation can be observed between regions of attached flow. Presence of adverse pressure gradient results in greater interaction between counter-rotating vortices, leading to their early breakup and higher vortex decay rate compared to the zero pressure gradient case. Further, it is seen from the simulations that the counter-rotating array of vortices does not move away from the wall even far downstream.

**Keywords:** Laminar separation bubble; Rectangular vortex generators; Direct numerical simulation; Immersed boundary method.

## NOMENCLATURE

$C_f$	skin friction coefficient	$u_m$	mean streamwise velocity
$C_p$	coefficient of pressure	$U_\infty$	free stream velocity at inlet
$D$	Spanwise spacing between VGs		
$d$	Spanwise blade spacing within VG	$\tau_w$	wall shear stress
$h$	VG blade height	$\delta$	boundary layer thickness
$p$	pressure	$\delta^*$	displacement thickness
rms	root mean square	$\delta_{in}^*$	displacement thickness at inlet
$Re_{\delta_{in}^*}$	Reynolds number based on displacement thickness at inlet and free stream velocity	$\theta$	momentum thickness
$u_\tau$	friction velocity	$\theta_s$	momentum thickness at separation

## 1. INTRODUCTION

In several low Reynolds number airfoil applications such as high altitude aircraft and compressor blades, laminar separation bubbles appear at angles of attack less than the stall angle. Small separation bubbles usually do not have much effect on the lift of an airfoil but a significant increase in drag may result due to thickening of turbulent boundary layer.

To delay or prevent their occurrence, momentum must be infused into the boundary layer enabling it to sustain the adverse pressure gradient. A laminar separation bubble was simulated by Singh and Sarkar (2011) by imposing suction at the upper boundary. In this study, the goal is to reduce or eliminate the laminar separation bubble, through the use of vortex generators. Though vortex generators are commonly used to control separation in

turbulent boundary layers, their use for this purpose in the laminar boundary layer is not very frequent. The vortex generator heights investigated numerically are  $0.33 \delta$  (case VG-1) and  $0.66 \delta$  (case VG-2). It should be noted that height of the vortex generators in the case VG-1 is close to the definition of submerged/low-profile VGs given by Lin (2002) while case VG-2 is closer to the definition of a conventional vortex generator. It is anticipated that streamwise vortices produced by the vortex generators will energize the near-wall retarded fluid to overcome the adverse pressure gradient, preventing or reducing the extent of separation. Further, their small height is not expected to cause any premature transition to turbulence.

The height of conventional, passive vortex generators (VGs),  $h$ , is of the order of boundary layer thickness,  $\delta$ . Such VGs have been in use since 1940s (Taylor, 1948a). These simple and effective devices consist of vanes of different shapes attached to the mounting surface. The vanes are usually placed at an angle to the oncoming flow. They generate embedded longitudinal vortices to transfer momentum to near-wall flow making use of micro-movements (Gad-el-Hak and Bushnell, 1991a). In the vortices, fluid with high streamwise momentum moves helically to mix with the slow-moving near-wall flow and replace it. Passive vortex generators have been applied to compressor blades, diffusers (Brown *et al.*, 1968) and airfoils (Pearcey, 1961; Bragg and Gregorek, 1987) etc. Research, both basic fluid-dynamic and applied, has been mainly experimental in nature and numerical simulations started appearing in the past decade only. Guidelines for conventional vortex generators can be found in papers by Taylor (1948b), Henry *et al.* (1956) and Pearcey (1961). Inviscid theory was applied by Pearcey (1961) to predict the cross-stream movement of vortices as they travel downstream. He also prescribed the optimum ratio for spanwise spacing ( $D$ ) to spanwise blade spacing within the pair ( $d$ ) as  $D/d \approx 4$  and the ratio of spanwise spacing to blade height ( $h$ ) as  $D/h \approx 10$ .

The conventional vortex generators have been used in varied forms, in the form of rectangular vanes, triangular vanes, backward or forward ramp, wishbones and doublets etc. Though rugged and low-cost, these devices produce considerable parasitic drag and the recent trend is to reduce the device height from  $O(\delta)$  to  $O(\delta/5)$  or less. This reduction in height significantly reduces the parasitic drag. It is made possible because of availability of required momentum levels close to the surface (Lin and Howard, 1989; Lin *et al.*, 1990; Gad-el-Hak and Bushnell, 1991b; Lin, 2002). However, the sub-boundary layer devices need to be placed relatively closer to the separation location and these are more suitable where the flow-separation line does not change its position appreciably. Wind tunnel tests were conducted by Kerho *et al.* (1993) to assess the performance of various types of submerged vortex generators in controlling the laminar separation bubble present on a low Reynolds number LA2573A airfoil. The

Reynolds numbers ranged from 200,000 to 600,000 and the angles of attack were less than the stall angle. An analytical study of three-dimensional turbulent flow triggered in a boundary layer by vortex generators mounted on the surface was carried out by Smith (1994). Analytical formulae were suggested by him for favourable vortex generator distributions.

Bender *et al.* (1999) used a new approach to model a vortex generator vane. In their analysis, they introduced a source term representing the side force produced by vanes. Hamstra *et al.* (2000) used the simplified model of VG vane given by Bender *et al.* (1999) to compare their simulation of vortex generator vanes with experimental results. Allan *et al.* (2002) numerically simulated a single VG vane and a vortex generating jet for flow over a flat plate. The height of their VG vane was just a fraction of the boundary layer thickness. Their computations involved the steady-state solution to the Reynolds-averaged Navier-Stokes equations. However, their simulations underestimated the initial magnitude of peak streamwise vorticity and its decay was poorly predicted. A more diffused vortex was generated by the numerical simulations. However, the vortex strength matched well with the experimental observations. A comprehensive review on deployment of low-profile vortex-generators can be found in Lin (2002).

Sohankar and Davidson (2003) performed direct numerical simulation and large-eddy simulations for resolutions up to 1.2 million points to examine the effect of vortex generators on the flow-field and heat transfer in a plate-fin heat-exchanger. Godard and Stanislas (2006) performed a detailed experimental study for optimization and characterization of passive vortex generators. They tabulated the optimal configuration for both co-rotating and counter-rotating devices and concluded that counter-rotating devices are more effective than the co-rotating ones. Shan (2007) used the immersed boundary method in conjunction with DNS to investigate the flow-field behind a pair of active vortex generators on a flat plate. Shan *et al.* (2008) numerically simulated subsonic flow separation over a NACA0012 airfoil. They investigated control of flow separation using both passive and active vortex generators. It was observed by them that the separation zone was completely eliminated by active vortex generators separation while the use of passive vortex generators led to a reduction in the averaged separation zone by more than 80%. Henze *et al.* (2011) have created a benchmark data set for flow-field and heat transfer characteristics in the presence of longitudinal vortices for a Reynolds number of 300,000. A number of investigations on different geometries of vortex generators, both experimental and numerical, have been carried out by Velte *et al.* (2007, 2013, 2014) to study vortex generator induced flow field and its effect on separation control.

In the present work, the IB method has been combined with DNS in Cartesian coordinates to model the vortex generators. Effect of vortex

generators of two different heights on separation control has been investigated. The counter-rotating vortices generated are characterized, while streamwise evolutions of non-dimensionalised maximum values of vorticity, vortex strength, wall-normal velocity and spanwise velocity are presented. One of the objectives of the work is to resolve the three-dimensional flow structures and correlate with turbulence evolved due to the vortex generators. Strong distortion of the normal two-dimensional boundary layer takes place due to the presence of longitudinal vortices created by the vortex generators. It is observed from the simulations that separation is delayed and the mean bubble length is significantly reduced in the first case (VG-1) while the original bubble is completely eliminated by the greater height vortex generator (case VG-2). However pockets of recirculating flow can be observed in this case between regions of attached flow.

## 2. NUMERICAL FORMULATION

### 2.1 Governing Equations

The incompressible mass and momentum equations are solved which can be given as,

$$\frac{\partial u_j}{\partial x_j} = 0 \quad (1)$$

and

$$\frac{\partial u_i}{\partial t} + \frac{\partial}{\partial x_j} (u_j u_i) = -\frac{\partial p}{\partial x_i} + \frac{1}{Re_{\delta_{in}^*}} \nabla^2 u_i + F_i \quad (2)$$

where,  $u_i$  represents the velocity field and  $Re_{\delta_{in}^*}$  is the Reynolds number based on displacement boundary layer thickness  $\delta_{in}^*$  and the inlet free stream velocity  $U_\infty$ . The presence of the body forces  $F_i$  is due to the immersed boundary method. In the present work direct forcing IB method with unidirectional quadratic interpolation of Muldoon & Acharya, (2005) is applied. Details of the numerical scheme can be found in Singh (2013).

### 2.2 Computational Details

The dimensions of the computational domain are the same as in previous simulation of laminar separation bubble (Singh and Sarkar, 2011) i.e.,  $L = 200 \delta_{in}^*$ ,  $W = 30 \delta_{in}^*$ ,  $H = 10 \delta_{in}^*$ . The placement of vortex generators in the domain is shown schematically in Fig. 1. The dimensions of the vortex generators have been chosen to lie within the parameters laid down by Pearcey (1961) and Lin (2002) for producing long-lasting vortices. The VG blades are mounted perpendicular to the flat plate with an angle of  $30^\circ$  to the incoming flow. The blade length ( $l$ ) is  $4 \delta_{in}^*$  for both the cases

The vortex generator thickness ( $t$ ) has been taken as  $0.1l$  while the vortex generator height is  $1.0 \delta_{in}^*$  in

the first case, denoted as VG-1 and  $2.0 \delta_{in}^*$  in the second case, denoted as VG-2. The distance between vortex blades at the mid-section ( $d$ ) is  $5.0 \delta_{in}^*$ , while the distance between two vortex generator pairs ( $D$ ) is  $15 \delta_{in}^*$ . Two pairs of rectangular VG blades have been placed in the laminar region, upstream of the location, where the flow separates in the uncontrolled case, the trailing edge being at  $x = 10.64 \delta_{in}^*$ . They have been arranged to generate counter-rotating vortices. It was shown by Godard and Stanislas (2006) that vortex generators generating counter-rotating vortices are more efficient than co-rotating ones by a factor of two. For the present study  $\delta_{in}^*$  is calculated as 8 mm while the boundary layer thickness at the location of vortex generators is 24 mm implying that the vortex generators have sub-boundary layer heights. The boundary conditions used at inlet, outlet, in flow normal direction and spanwise direction are discussed below.

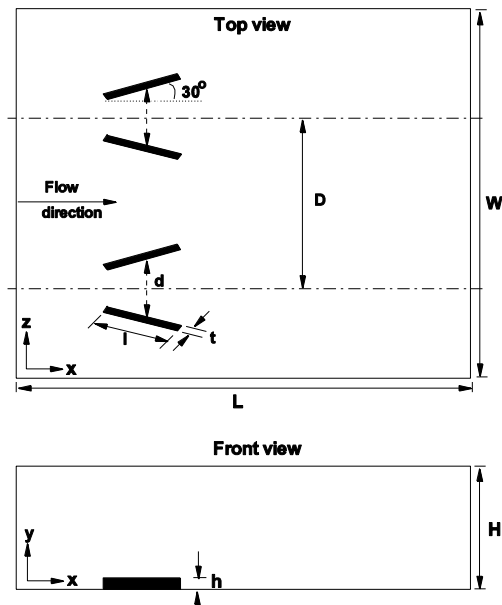


Fig. 1. Schematic of computational domain showing the placement of vortex generators (not to scale).

At the inlet, a Blasius velocity profile is specified for  $u$  corresponding to  $Re_{\delta_{in}^*} = 500$ , while  $v = w = 0$ .

A convective boundary condition (Orlanski, 1976) is imposed at the outlet, which can be written as

$$\frac{\partial u_i}{\partial t} + U_c \frac{\partial u_i}{\partial x_c} = 0 \quad (3)$$

Here, subscript  $c$  denotes the direction normal to the outflow boundary.  $U_c$ , the convective velocity is considered to be constant across the outflow boundary and is fixed at each time step by averaging the velocity normal to the boundary over a transverse plane.

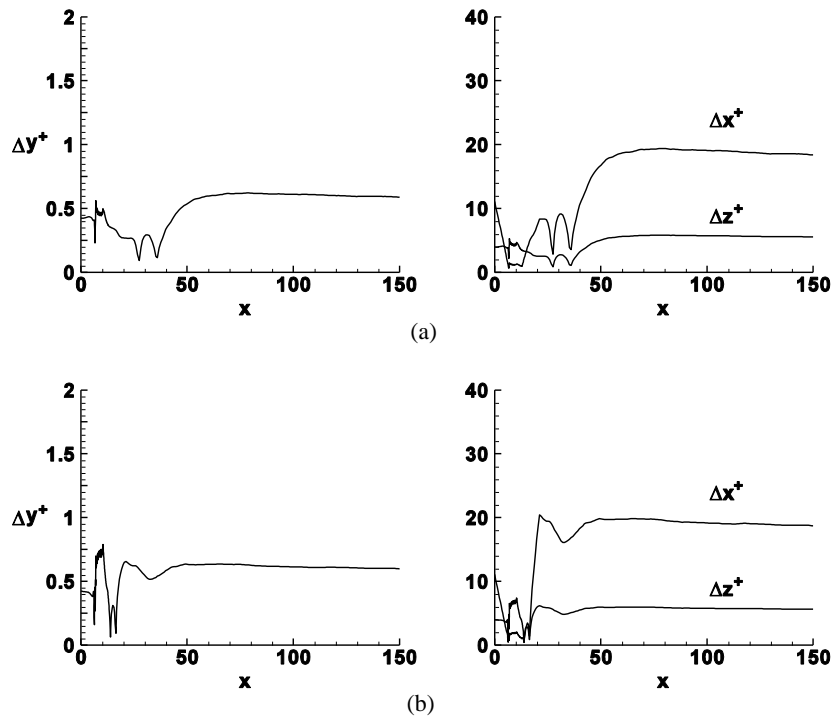


Fig. 2. Near wall grid resolutions in wall units for (a) case *VG-1* and (b) case *VG-2*.

On the lower boundary a no-slip condition is applied i.e.  $u = v = w = 0$ . At the upper boundary,  $u = 1.0$  and  $v = w = 0$  and a suction profile following the Gaussian distribution of the wall-normal velocity component has been specified. The expression of the suction-velocity distribution, following Alam and Sandham (2000) is given by,

$$S(x) = a_s \exp[-b_s(x - c_s)^2] \quad (4)$$

The values of constants are given in the Table 1.

**Table 1 Numerical parameters of suction and forcing profile**

$a_s$	$b_s$	$c_s$	$a_f$	$b_f$	$c_f$	$\omega$	$\beta$
0.15	0.02	25	$30.08^{-3}$	0.125	5	0.15	0.41

As naturally occurring disturbances are non-existent in numerical simulations, a disturbance strip applied upstream of separation triggers the transition of shear layer. The disturbance strip is applied to the normal velocity by the function given below, following Alam and Sandham (2000).

$$v'(x, z, t) = a_f \exp[-b_f(x - c_f)^2] \sin(\omega t) \sin(\beta z) \quad (5)$$

The constants  $a_f$ ,  $b_f$  and  $c_f$  controlling the disturbance are given in the Table 1. The flow is assumed to be homogeneous in the spanwise direction, hence a periodic boundary condition is applied to all the velocity components in the spanwise direction.

The solver used here has been validated in previous

studies (Sarkar and Sarkar, 2009) on transitional and turbulent flows. The computational domain is divided into  $356 \times 128 \times 128$  cells along  $x$ ,  $y$  and  $z$  directions respectively. In the streamwise direction, a very fine uniform mesh is used around the vortex generators to get adequate number of immersed-boundary points on the vortex generator surface. Moving away from the vortex generators, the mesh is slowly stretched out till the beginning of the region where the bubble is expected. Thereafter the mesh is kept uniform till the end of the useful region. In the wall-normal direction, near the wall, a very fine uniform mesh is employed to resolve the flat-plate boundary layer and its interaction with the vortex generators: a slow stretching being employed thereafter. In the spanwise direction, a uniform fine mesh is used. It may be noted that since the vortex generator has a small thickness, use of a fine mesh in the spanwise direction is necessary to obtain adequate number of immersed-boundary points along the vane thickness.

Figure 2 shows the grid-resolutions along the wall. In the wall-normal direction,  $\Delta y^+$  fluctuates around 0.6, indicating a well-resolved viscous sub-layer. Near the vortex-generators,  $\Delta x^+$  is around 1.2 wall units. The value of  $\Delta z^+$  fluctuates around 6 wall units. Thus the grid-resolution everywhere in the domain is comparable to or better than the resolution employed in other such studies.

The time-step  $\Delta t$  for solution advancement is 0.02 in dimensionless units. Around 10000 iterations are needed for one flow pass. Initially, seven flow passes with wall disturbances are allowed for the evolution of flow. Statistics are taken for further ten flow passes after the flow reaches dynamic stability. The simulation took about 700 hrs on an Intel Xeon,

2.6 GHz, quad-core, twin processor machine with 16 GB RAM.

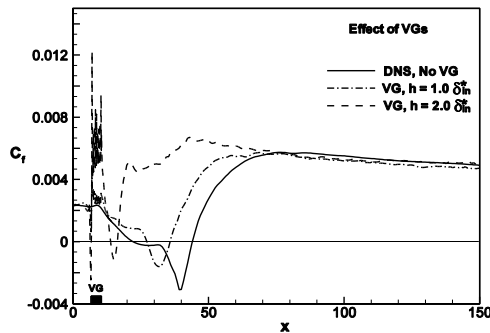


Fig. 3. Variation of mean  $C_f$ . The placement of VGs is also shown.

### 3. RESULTS AND DISCUSSION

#### 3.1 Mean Flow Characteristics

In this section the time- and span-averaged quantities are discussed. Spanwise variation of the flow quantities is considered in the next section

##### 3.1.1 Bubble Length

Evaluation of the vortex generator effectiveness can be best made by the reduction in the length of the mean separation bubble, brought about by the vortex generator. Figure 3 depicts the variation of mean skin friction coefficient along streamwise direction. The zero-crossings readily provide the mean separation and reattachment points. In the uncontrolled case the separation starts at  $x-x_i = 10.8$  and reattachment takes place at  $x-x_r = 33.4$ , implying a bubble length of 22.2, while for case *VG-1* separation point is at 16.6 and reattachment takes at 25.2 implying delayed separation and a reduction in bubble length by 62%. For the case *VG-2*, the original separation bubble is completely eliminated while a small vortex generator induced bubble can be seen downstream the vortex generators. The separation starts at  $x-x_i = 3.2$  and the flow reattaches at  $x-x_r = 5.8$  indicating that the bubble length is 2.6. Further investigations reveal the existence of very tiny bubbles within the vortex generator region itself.

##### 3.1.2 Coefficient of Pressure

The evolutions of mean coefficient of pressure  $-C_p$  along the  $x$  direction are compared in Fig. 4 for the cases *VG-1* and *VG-2* with the no vortex generator case. The presence of vortex generators causes a strong favourable pressure gradient depicted by a steep rise locally in  $-C_p$  in the vortex generator region. This is followed by a steep rise in pressure i.e. an adverse pressure gradient. As expected, both the rise and fall in the value of  $-C_p$  are much steeper in the case of greater VG height. It is observed that the plateau region is significantly reduced by the presence of vortex generators

#### 3.1.3 Mean flow Structure

Figure 5 shows the contours of mean streamwise velocity  $u_m$ , revealing the shape of the bubble for the two VG heights. In the contour plots, the point of separation is marked as *S* and reattachment as *R*. It is seen that vortex generator of smaller height considerably reduces the extent of bubble without causing excessive disturbance to the flow. while the greater height vortex generator perturbs the flow enough to cause early transition. A zoomed view of the section where vortex generators are present is also presented for the case *VG-2*. It shows the existence of tiny bubbles near the VG leading edge too in addition to the downstream bubble. It is evident from the figure that the presence of VGs of greater height excessively perturbs the flow and results in greater thickening of the boundary layer as compared to the other case.

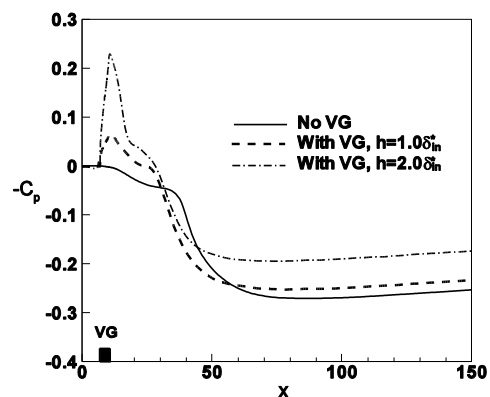
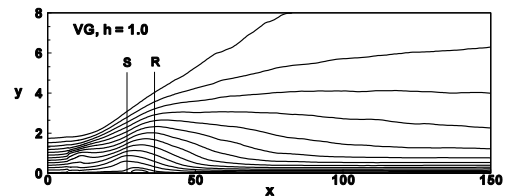
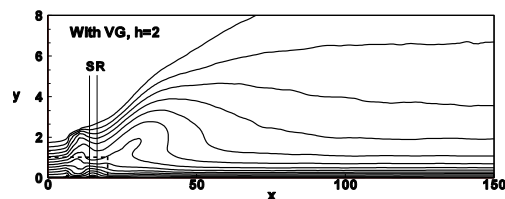


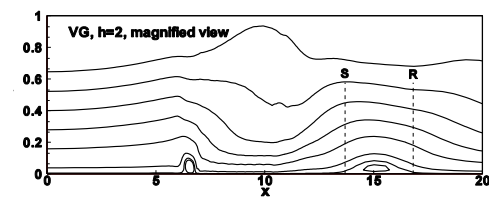
Fig. 4. Evolution of wall pressure-coefficient for different cases.



(a)



(b)



(c)

Fig. 5. Contours of mean streamwise velocity for (a) case *VG-1* and (b) *VG-2*. A zoomed view of the marked region for *VG-2* is shown in (c).

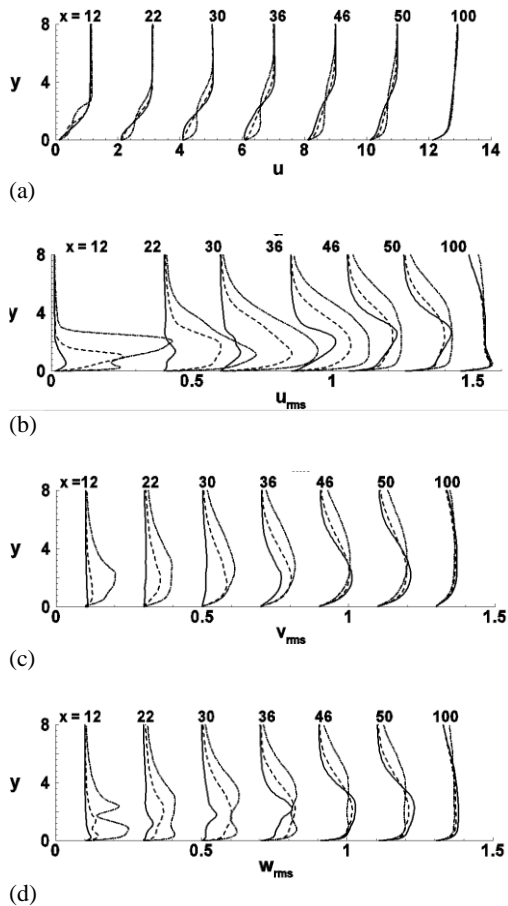


**Fig. 6. Profiles of (a)  $u_m$  (b)  $u_{rms}$  (c)  $v_{rms}$  and (d)  $w_{rms}$  at different streamwise locations. Solid line: No VG; dashed line: case VG-1, dash-dotted line: case VG-2.**

Figure 6(a) compares the mean streamwise velocity component and Figs. 6(b)-(d) compare the r.m.s. of streamwise, wall-normal and spanwise velocity fluctuations respectively obtained from the cases VG-1 and VG-2 with the uncontrolled case. The horizontal axis of the figures is arbitrarily chosen to represent the variation in magnitude of the variables with respect to the change in position along the streamwise direction. Figure 6(a) illustrates the differences in growth of the shear layer, separation bubble with a flow reversal and the reattachment. After the reattachment, the separated shear layer relaxes downstream towards an equilibrium turbulent boundary layer in all the three cases. Up to  $x = 50$  the value of mean streamwise velocity near the wall is larger in the case VG-2 as compared to the other two cases, while away from the wall it is smaller in comparison. This may be attributed to the strong churning motion created by the vortices in the case VG-2. Figures 6(b)-(d) indicate the evolution of turbulence after the separation. In the controlled cases, the growth of perturbations starts just downstream of the vortex generator trailing edge. The magnitude of perturbations is much larger in the case VG-2, for example the maximum magnitude of  $u'$  is 45% of the inlet free-stream velocity in the case VG-2 while for the case VG-1, it is 25% of the inlet free-stream velocity

### 3.2 Time-Averaged Flow

The time-averaged quantities, which are function of the three spatial directions, are discussed in this section.

#### 3.2.1 Wall Shear-Stress

Figure 7 shows the downstream development of wall shear stress at five spanwise positions indicated in the figure. The locations  $P_1$  and  $P_3$  are close to the VG blades' trailing edges,  $P_2$  is at the symmetry line between the two blades,  $P_5$  is at the symmetry line between the two pairs and  $P_4$  is in between  $P_3$  and  $P_5$ . It can be inferred from the figures that the three-dimensionality in shear stress, introduced by the vortex generators begins to die down by  $x = 30$  in the case of smaller VG height, while the flow continues to exhibit three-dimensional character up to  $x = 70$  for the case of larger height vortex generator. This is in contrast to the previous case without suction, where the three-dimensionality persisted longer in the case of lower height VG. The figures also reflect the initial increase in wall shear-stress due to the presence of vortex generators, compared to the uncontrolled case.

#### 3.2.2 Time-Averaged Bubble

Time-averaged streamwise velocity contours and streamlines for the two cases have been plotted in Figs. 8(a) and 8(b) at five spanwise locations to investigate the variation of bubble shape and size in the spanwise direction. The mean time- and span-averaged bubble is also superimposed for comparison. For the smaller height i.e. VG-1, at locations  $P_1$  and  $P_3$  which are close to the trailing edges of VG blades, the extent of separation is considerably larger as compared to other spanwise locations.

At these locations, instead of one large bubble, several small bubbles are seen, the first one sticking to the vortex generator edge itself. However for the larger height  $h = 2$ , the extent of separation at these locations is quite small, the figure showing only a single bubble clinging to the VG edges. At location  $P_2$ , (midway between the two vanes of vortex generator) no separation bubble exists in the smaller height VG case while a small bubble is seen in the other case. At the other two locations  $P_4$  and  $P_5$  lying between the two VG pairs, presence of a single large separation bubble is seen at both the locations in the case of smaller height VG while no bubble is detected at the location  $P_4$  for the case VG-2. Figures 9(a) and 9(b) show the top view of the time-averaged reversed flow regions for the two cases. These further confirm the above-mentioned observations about spanwise extent of the bubbles.

#### 3.2.3 Velocity Field and Vortex Development

Figures 10(a) and 10(b) show mean streamwise velocity profiles at four spanwise locations for the two VG heights. Location 1 is between vanes of a VG, location 2 is at the symmetry-line between the two VG pairs, location 3 is exactly downstream of

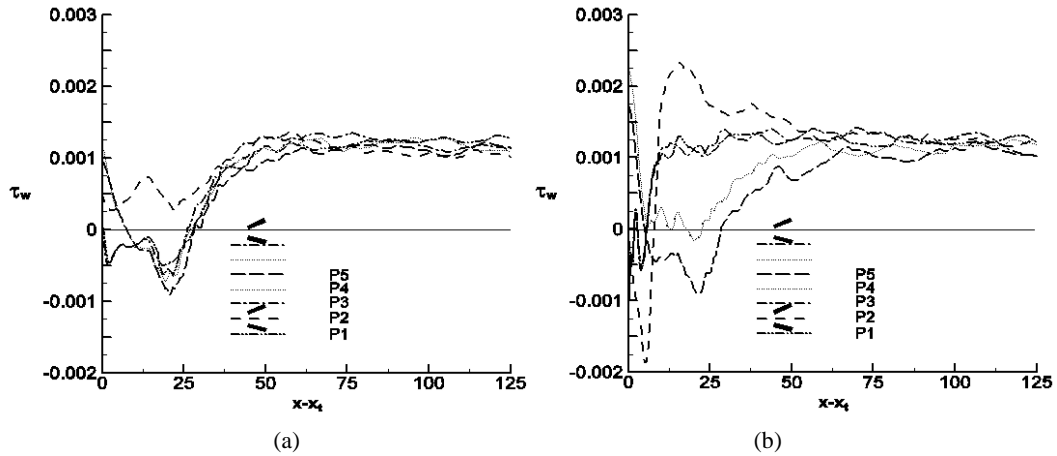


Fig. 7. Time-averaged wall shear stress at different spanwise locations for (a) case *VG-1* and (b) case *VG-2*.

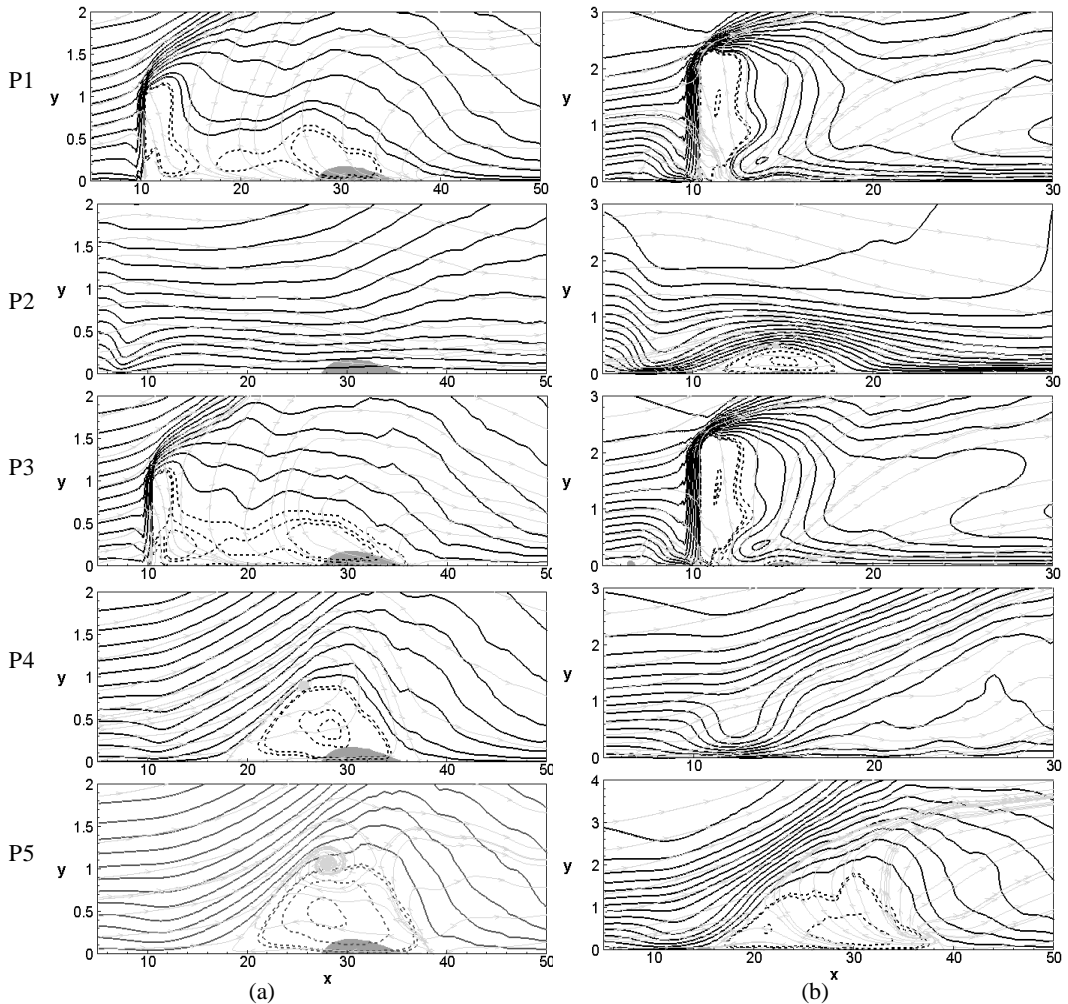
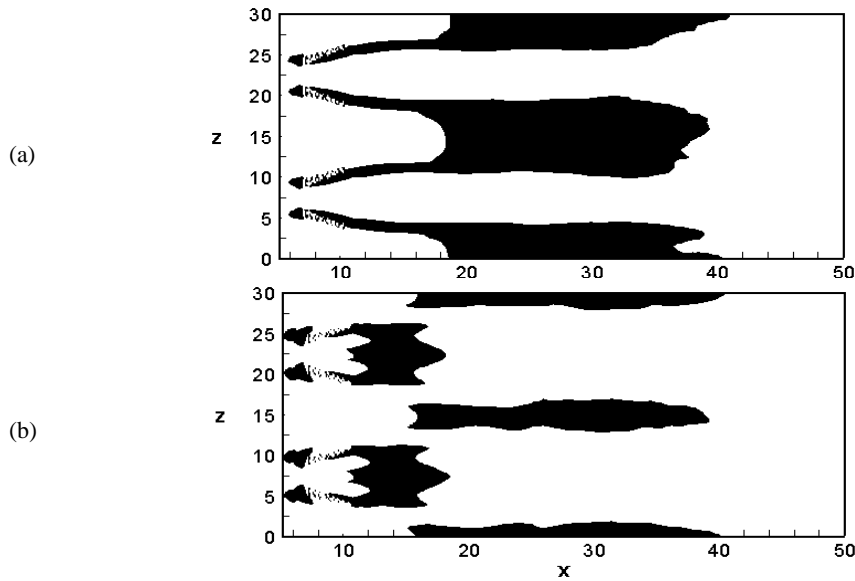


Fig. 8. Time-averaged streamwise velocity contours and streamlines at different spanwise locations for (a) case *VG-1* and (b) case *VG-2*. Mean reversed flow (grey shaded) is also superimposed.

VG blade and location 4 is mid-way between 2 and 3. It can be immediately recognized that location 3 produces maximum velocity deficit in the case *VG-1*. In the case of greater VG height (*VG-2*), the  $u$ -velocity profiles are S-shaped at locations 2 and 3

indicating higher values of  $u$ -velocity near the wall and in the outer region while lower values in-between. As expected, in the case *VG-1*, the distortion of profiles is much less severe. Negative  $u$ -velocity signifying reversed flow is observed at



**Fig. 9. Top view of the spanwise extent of time-averaged bubble for (a) case VG-1 and (b) case VG-2. Dark colour indicates regions of reversed flow.**

spanwise location 3 at all streamwise locations for the case VG-1 while reversed flow is indicated only at  $x/h = 5.5$  and 9 for the case VG-2.

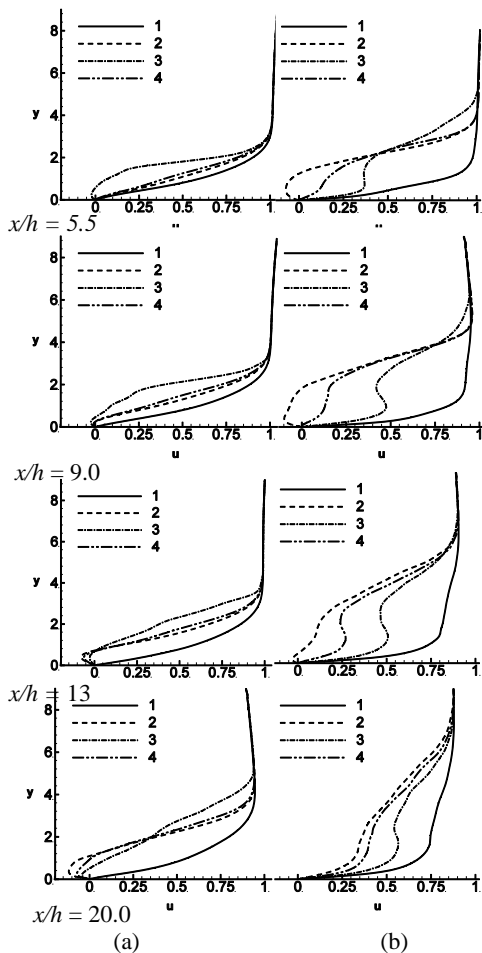


**Fig. 10. Profiles of time-averaged streamwise velocity at different spanwise locations, for (a) case VG-1 and (b) VG-2.**

Figures 11(a) and 11(b) show the time-averaged streamwise velocity ( $u$ ) contours in the  $y$ - $z$  plane at  $x/h = 5.5, 9, 13$  and 20 for both the vortex generator heights; the in-plane secondary velocities also shown as vectors. The strong thinning effect of vortex generators on the boundary layer in the downwash region where high-momentum fluid is being transferred into the near-wall region is clearly visible. At the same time, in the upwash region, the thickening of boundary layer takes place due to transfer of low momentum fluid. It is also seen that the thinning effect is reduced as the vortex moves downstream.

Contours of time-averaged streamwise vorticity ( $\omega_x$ ) are depicted at four spanwise locations in Figs. 12(a) and 12(b) from where it can be seen that the vortices grow larger but become weaker as they move downstream. The no-slip condition causes a strong shear leading to induction of a region of vorticity of opposite sign in the near-wall region. As expected, vortices generated in case VG-2 are stronger and larger in extent.

### 3.3 Instantaneous Flow and Three-Dimensional Structure

In this section, development of three-dimensional motions and breakdown to turbulence are discussed in brief. Contours of instantaneous streamwise velocity at different sections are presented for the two VG cases, illustrating important features of the flow field. Figures 13(a) and 13(b) show contours of instantaneous streamwise velocity in two  $x$ - $y$  planes (at  $z = 7.5$  and  $z = 15$ ) at a particular time instant, for the cases VG-1 and VG-2 respectively. The location  $z = 7.5$  is between the two blades of vortex generator while  $z = 15$  is the plane of symmetry between the two vortex generators. The flow structure at  $z = 15$  is similar to that of the uncontrolled case while at  $z = 7.5$  it is markedly different showing no trace of reversed flow. A small

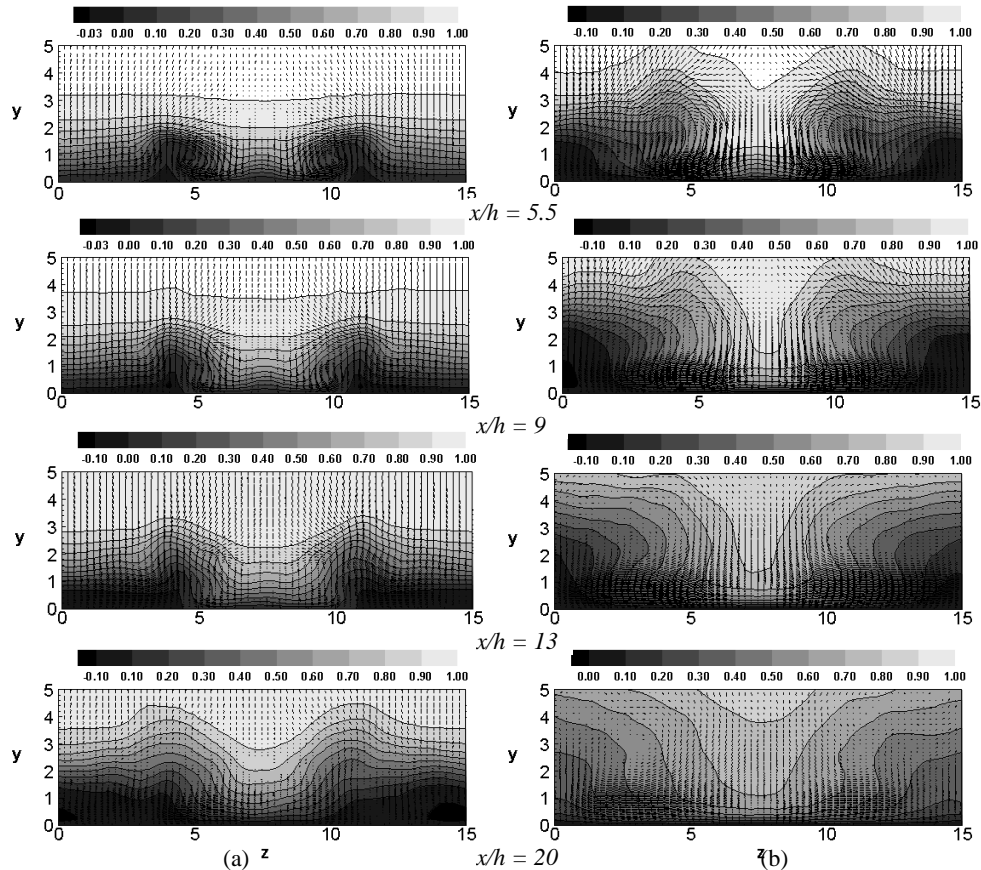


**Fig. 11. Time-averaged streamwise velocity contours in  $y$ - $z$  planes at different streamwise locations for (a) case  $VG-1$  and (b) case  $VG-2$ . Secondary flow vectors are also superimposed.**

bubble is visible from  $x = 11.0$  to  $x = 18.0$  for the case  $VG-2$ . Figures 14(a) and 14(b) show the top view ( $x$ - $z$  plane) of streamwise velocity contours obtained from the two case  $VG-1$  and  $VG-2$  respectively for two wall normal location ( $y = 0.05$  and  $0.1$ ). It is observed that longitudinal vortices generated by the smaller height VG do not show any tendency to diverge after leaving VG trailing edge; this effect may be attributed to the imposed suction as the vortices show significant spanwise motion in the case without suction. However, the stronger vortices generated by the VG of greater height are not affected much. They tend to follow the direction in which the VG blade is aligned and show significant spanwise divergence due to strong interaction between the vortices. The top-view illustrates that the initial flow-field is two-dimensional and the boundary layer separates as laminar.

Figures 15(a) and 15(b) show the side views ( $y$ - $z$  plane) of streamwise velocity contours for eight streamwise sections at the same time. Location  $x = 13.5$  is slightly downstream the VG trailing edge. Formation and growth of vortices can be seen as we move downstream. Bigger and stronger vortices are formed in the case  $VG-2$ . Two-dimensionality is preserved till  $x = 15$  and only a slight distortion is seen at  $x = 20$  in the case  $VG-1$  while the spanwise asymmetry starts setting in as early as  $x = 13.5$  and vortices can no longer be identified beyond  $x = 15$

for the case  $VG-2$ . In both the cases, thinning of the boundary layer in the downwash region and thickening of the upwash region are clearly seen. As expected these effects are more pronounced for the case  $VG-2$ . The iso-surfaces of instantaneous streamwise vorticity for the two cases are presented in Figs. 16(a) and 16(b) respectively. Figures 16(a) and 16(b) illustrate the development of longitudinal vortices downstream of vortex generators and their breakup leading to small scale structures and turbulence. These figures show the effect of imposed suction very clearly. In the case  $VG-1$  the flow is three-dimensional only in the region of vortices and then there is a sudden breakdown to small-scale structures around  $x = 30$ . However, it is difficult to make any comment about the mechanism of transition. The imposition of adverse pressure gradient forces greater interaction between the counter-rotating vortices leading to early breakup and increased vortex decay as compared to the no-suction case. A similar effect has been reported by Ashill *et al.* (2002) too.

### 3.4 Turbulence Statistics

Figures 17(a) and 17(b) depict the mean evolution of peak r.m.s. values of velocity fluctuations. The figures illustrate that downstream of VGs, the turbulence intensity in the case  $VG-1$  is about 25% while in case  $VG-2$  it is 45%. These values of turbulence intensity are similar to those obtained for the no-suction case. However, in this case as the

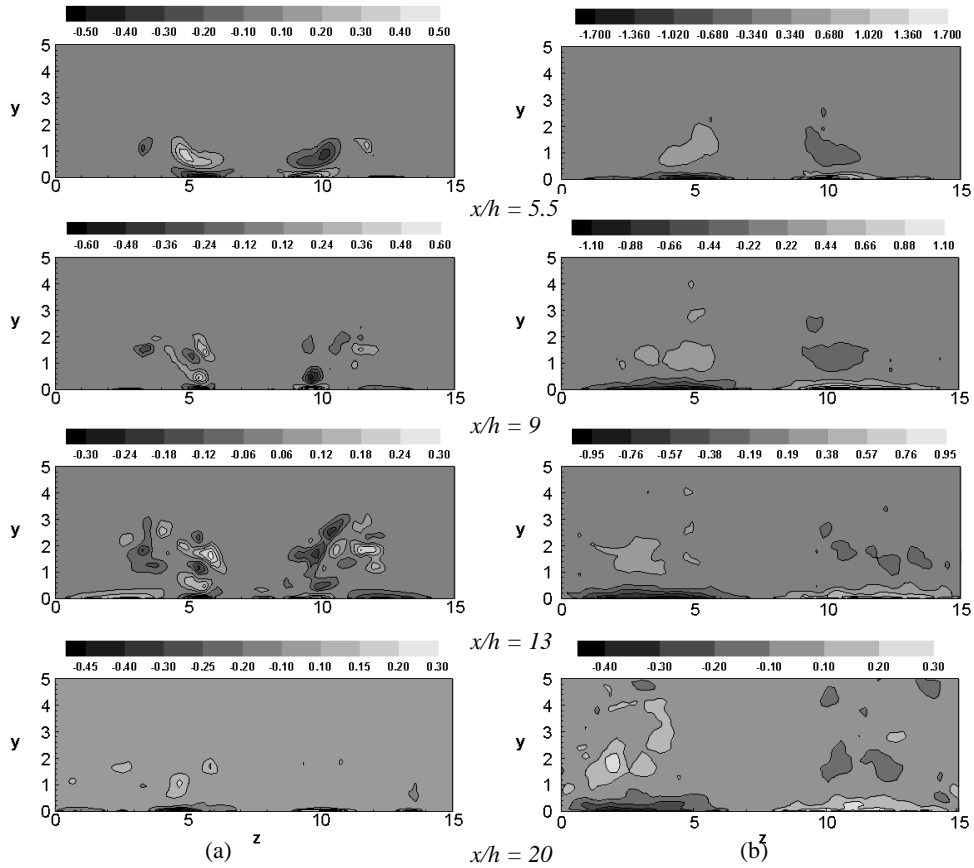


Fig. 12. Time-averaged streamwise vorticity contours in  $y$ - $z$  planes at different streamwise locations for (a) case *VG-1* and (b) case *VG-2*.

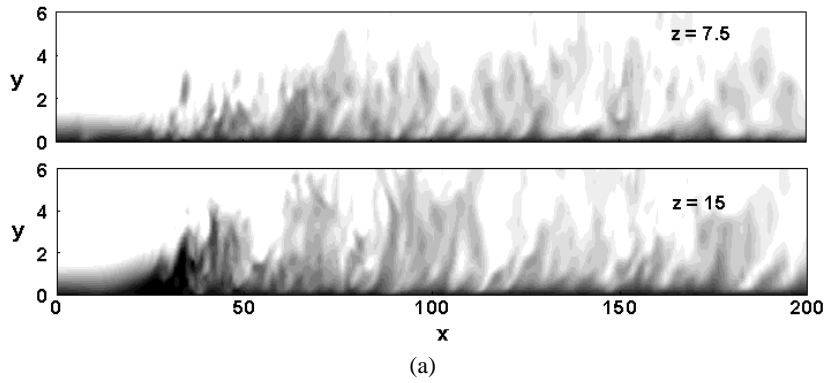


Fig. 13. contd.

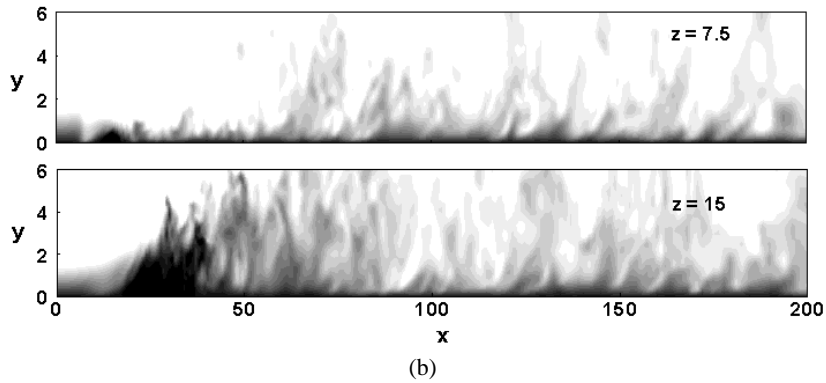
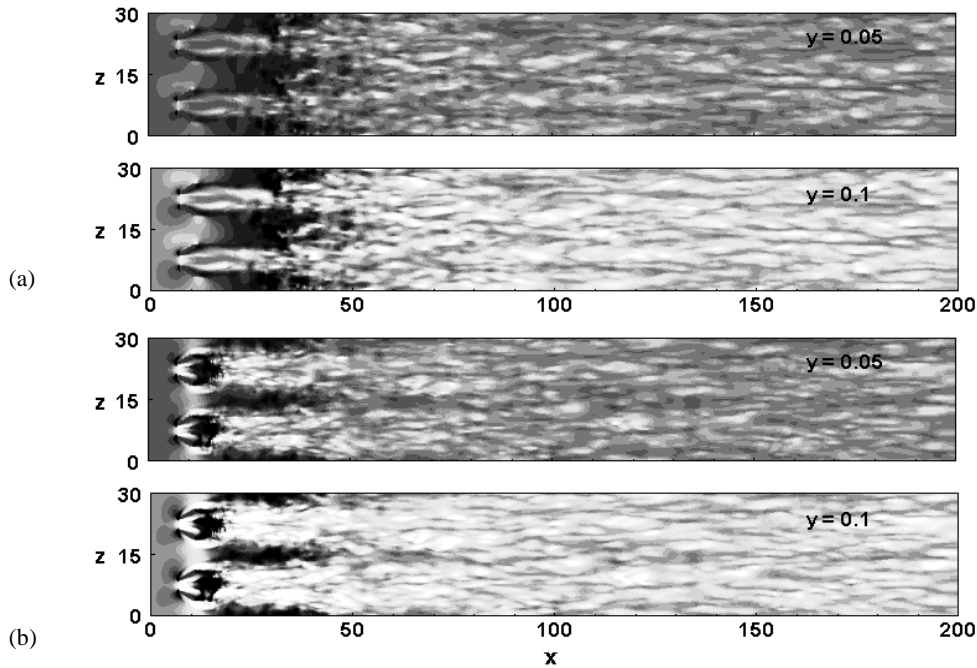
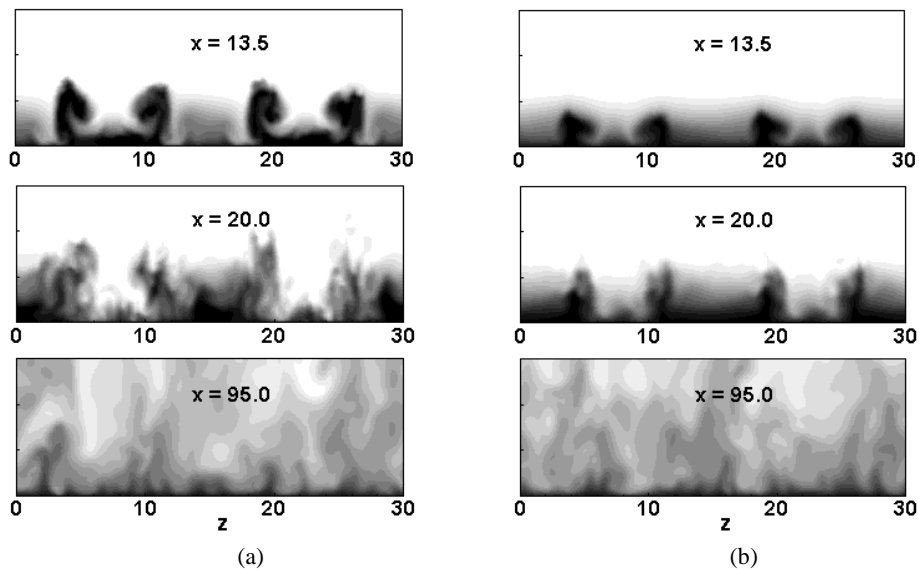


Fig. 13. Instantaneous contours of streamwise velocity in  $x$ - $y$  planes at  $z = 7.5$  and  $15.0$  for (a) case *VG-1* and (b) case *VG-2*. Maximum level is  $0.91$ , minimum level is  $-0.002$  with  $13$  levels in between.



**Fig. 14.** Instantaneous contours of streamwise velocity in  $x$ - $z$  planes at  $y = 0.05$  and  $0.1$  for (a) case *VG-1* and (b) case *VG-2*. Maximum contour level is  $0.91$ , minimum level is  $-0.002$  with  $13$  levels in between.



**Fig. 15.** Instantaneous contours of streamwise velocity in  $y$ - $z$  planes at  $x = 13.5, 20.0,$  and  $95.0$  for (a) case *VG-1* and (b) case *VG-2*. Maximum level is  $0.91$ , minimum level is  $-0.002$  with  $13$  levels in between.

flow evolves, slightly lower values of turbulence intensity of about 12% are observed compared to the value of about 15% in the no-suction case. This may be attributed to the imposition of suction.

The contours of Reynolds stresses for the cases *VG-1* and *VG-2* are presented in Figs. 18(a) and 18(b) respectively. The maxima for the stresses are concentrated in the region just downstream the trailing edge of the vortex generators. However the magnitude of stresses in the case *VG-2* is 3 to 5 times larger than that in the case *VG-1*. Contours of turbulent kinetic energy (TKE) and the production

(PKE) are depicted in Fig. 19(a) and 19(b) respectively. The maximum production occurs just downstream the vortex generators. As production occurs in the region of high turbulence stress and high spatial velocity gradient, aligned in the same direction, high production in this region can be attributed to concentration of relatively large-scale vortices. However for the case *VG-2*, high levels of production are again seen at  $x = 16.8$ , just after the reattachment and then the value of production progressively decreases for downstream sections. The near wall character appears far downstream of reattachment

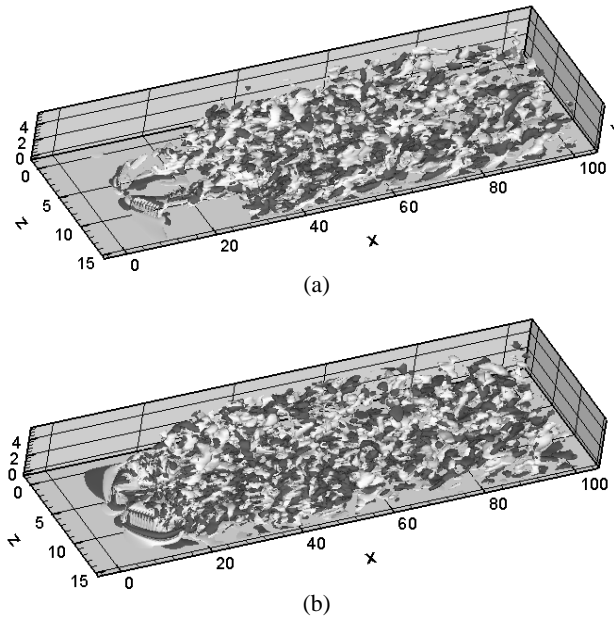


Fig. 16. Iso-surfaces of instantaneous streamwise vorticity for (a) case *VG-1*, contour levels are -0.15 and 0.15 (b) case *VG-2*, contour levels are -0.1 and 0.1.

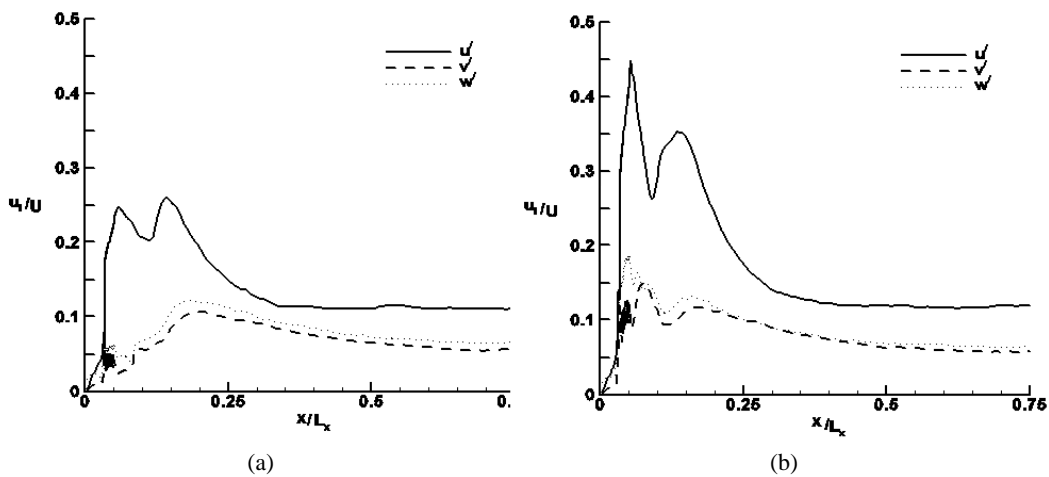


Fig. 17. Mean profiles of maximum r.m.s. values of velocity components ( $u'$ ,  $v'$ ,  $w'$ ) along the streamwise direction for (a) case *VG-1* (b) case *VG-2*.

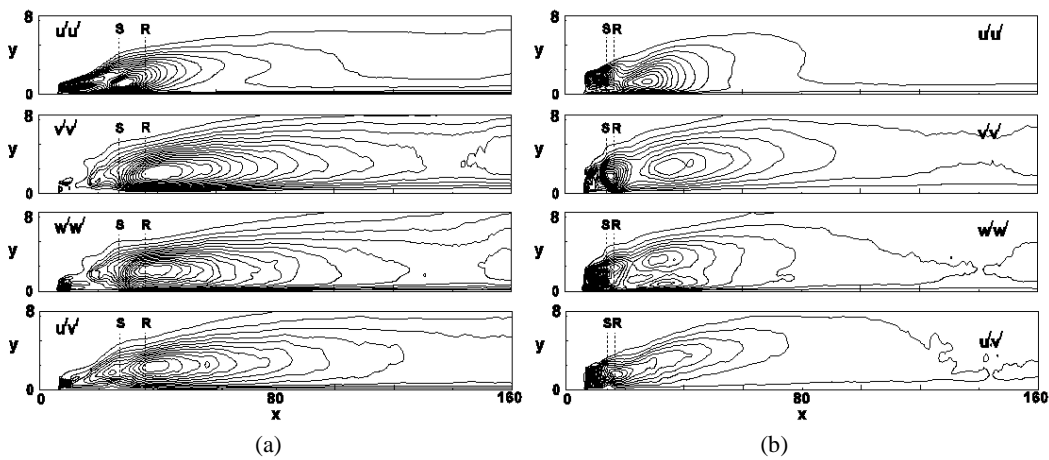


Fig. 18. Contours of fluctuation statistics,  $\overline{u'u'}$ ,  $\overline{v'v'}$ ,  $\overline{w'w'}$  and  $\overline{u'v'}$  for (a) case *VG-1*, maximum contour levels are 0.067, 0.012, 0.015 and 0.0037 respectively; (b) Case *VG-2*, maximum contour levels are 0.199, 0.025, 0.034 and 0.012 respectively.

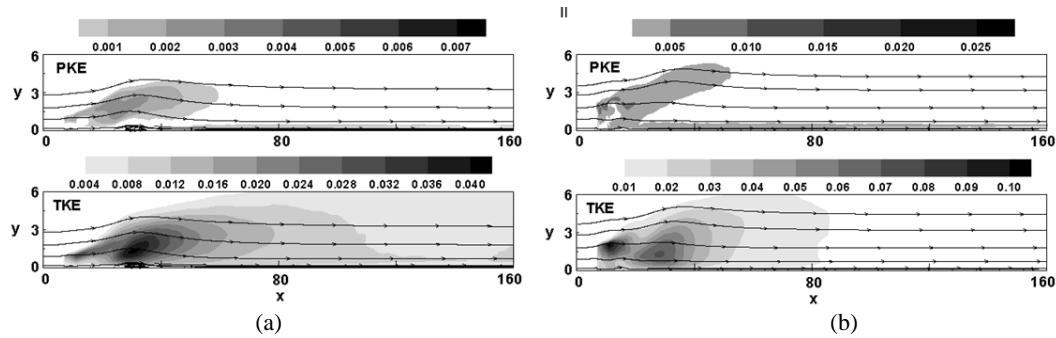


Fig. 19. Contours of mean TKE and PKE for (a) case VG-1 and (b) case VG-2.

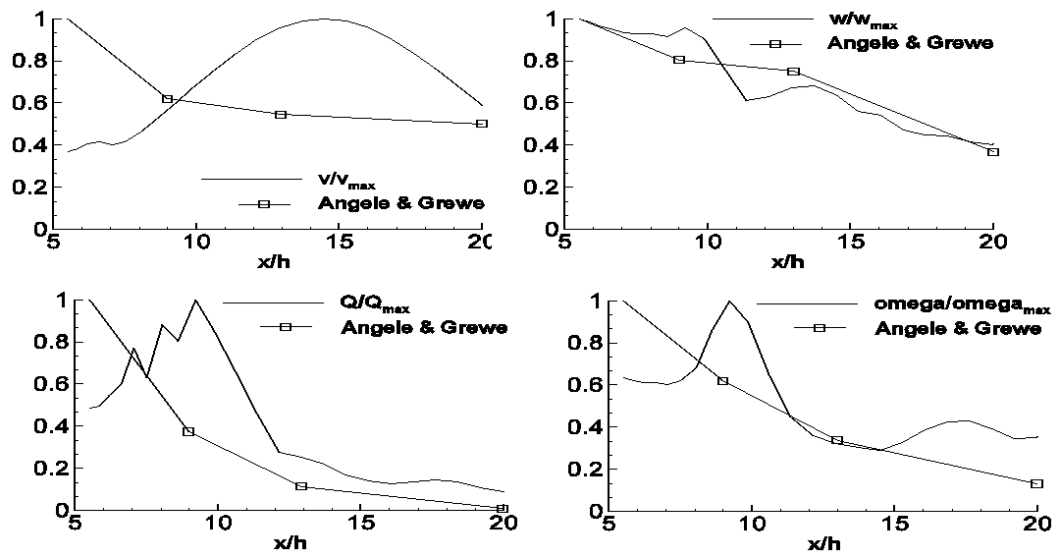


Fig. 20. Comparison of present simulation (case VG-1) with experimental data of Angele and Grewe (2007).

### 3.5 Comparison with Experimental Data

Results from the present simulations have been compared with the experimental data obtained by Angele and Grewe (2007) in Fig. 20. It may be noted that their vortex generator geometry and experimental conditions do not closely match those of the present simulation. The quantities  $v/v_{max}$  and  $w/w_{max}$  closely follow the experimental observations of Angele and Grewe (2007) while  $Q/Q_{max}$  and  $\omega/\omega_{max}$  show general agreement with the trend of decay. It may be noted that the quantities without subscript, denoting their maximum value in the  $y$ - $z$  plane at a particular  $x$ -location, have been non-dimensionalized by their respective maximum values in the  $y$ - $z$  plane at  $x/h = 5.5$  denoted by the subscript 'max'.

## 4. CONCLUSIONS

In this study, the performance of sub boundary layer vortex generators and conventional vortex generators in controlling the separation bubble has been compared. The evolution of the resultant highly three-dimensional flow has been studied. Two pairs of vortex generators mounted symmetrically along the spanwise direction are

placed upstream of separation point to produce counter-rotating vortices. Effect of these three-dimensional vortex generators of two different heights,  $0.33 \delta$  and  $0.66 \delta$  on the flow characteristics has been examined. The simulations show that the length of the separation bubble is reduced by sixty two per cent due to the deployment of vortex generators of height  $0.33 \delta$  while the original separation bubble is completely eliminated by the vortex generators of height  $0.66 \delta$ . The flow just downstream of vortex generators is highly three-dimensional and pockets of recirculating flow are interspersed with regions of attached flow. The iso-surfaces of instantaneous flow quantities along with turbulence statistics illustrate that flow becomes homogeneous in the spanwise direction downstream of vortex generators with enhanced levels of turbulence. Downstream of VGs, the turbulence intensity in the case VG-1 is about 25% while in case VG-2 it is 45%. These values of turbulence intensity are similar to those obtained for the no-suction case. However, as the flow evolves towards homogeneous turbulence, slightly lower values of turbulence intensity of about 12% are observed downstream compared to the value of about 15% in the no-suction case. It appears that the presence of adverse pressure gradient results in

greater interaction between counter-rotating vortices leading to their early breakup and higher vortex decay rate compared to the zero pressure gradient case. Further, it is seen from the simulations that the counter-rotating array of vortices does not move away from the wall even far downstream.

## REFERENCES

- Alam, M. and N. D. Sandham (2000). Direct numerical simulation of 'short' laminar separation bubbles with turbulent reattachment. *Journal of Fluid Mechanics* 403, 223–250.
- Allan, B. G., C. S. Yao and J. C. Lin (2002). Numerical simulation of vortex generator vanes and jets on a flat plate. *1<sup>st</sup> AIAA Flow Control Conference*, St. Louis MO, AIAA paper 02-3160.
- Angele, K.P. and F. Grewe (2007). Instantaneous behaviour of streamwise vortices for turbulent boundary layer separation control. *Journal of Fluid Engineering* 129, 226-235.
- Bender, E. E., B. H. Anderson and P. J. Yagle (1999). Vortex generator modelling for Navier-Stokes codes. *Third ASME/JSME Joint Fluids Engineering Conference*, ASME paper FEDSM99-6919.
- Bragg, M. B. and G. M. Gregorek (1987). Experimental study of airfoil performance with vortex generators. *Journal of Aircraft* 24, 303-309.
- Brown, A. C., H. F. Nawrocki and P. N. Paley (1968). Subsonic diffusers designed integrally with vortex generators. *Journal of Aircraft* 5(3), 221-229.
- Gad-el-Hak, M. and D. M. Bushnell (1991a). Separation control: Review. *ASME Journal of Fluids Engineering* 113, 5-30.
- Gad-el-Hak, M. and D. M. Bushnell (1991b). Status and outlook of flow separation control. *AIAA Paper No. 91-0037*, New York.
- Godard, G. and M. Stanislas (2006). Control of a decelerating boundary layer. Part 1: Optimization of passive vortex generators. *Aerospace Science and Technology* 10, 181-191.
- Hamstra, J. W., D. N. Miller, P. P. Truax, B. H. Anderson and B. J. Wendt (2000). Active inlet flow control technology demonstration. *ICAS-2000-6.11, 22nd International congress of the aeronautical science.*, Harrogate, UK.
- Henry, J. R., C.C. Wood and S. W. Wilbur (1956). Summary of subsonic diffuser data. *NACA RML-56F05*, Washington, DC.
- Henze, M., J. Wolfersdorf, B. Weigand, C. F. Deitz and S. O. Neumann (2011). Flow and heat transfer characteristics behind vortex generators - A benchmark dataset. *International Journal of Heat and Fluid Flow* 32, 318-328.
- Kerho, M., F. Hutcherson, R.F. Blackwelder and R. F. Liebeck (1993). Vortex generators used to control laminar separation bubbles. *Journal of Aircraft* 30(3), 315-319.
- Lin J.C. (2002). Review of research on low-profile vortex generators to control boundary-layer separation. *Progress in Aerospace Sciences* 38, 389-420.
- Lin, J. C. and F. G. Howard (1989). Turbulent flow separation control through passive techniques. *AIAA 2nd Shear Flow Conference*, Tempe AZ, AIAA paper 89-0976.
- Lin, J. C., F. G. Howard and G. V. Selby (1990). Small submerged vortex generators for turbulent flow separation control. *AIAA Journal of Spacecraft* 27(3), 503-507.
- Orlanski, I. (1976). Simple boundary condition for unbounded hyperbolic flows. *Journal of Computational Physics* 21, 251-269.
- Pearcey, H. H. (1961). Shock induced separation and its prevention by design and boundary layer control. In G.V. Lachmann (Ed.), *Boundary Layer and flow Control, Its Principle and Applications*, Vol. 2, Pergamon press, Oxford, 1166-1344.
- Sarkar, S. and S. Sarkar (2009). Large-Eddy Simulation of Wake and Boundary Layer Interactions Behind a Circular Cylinder. *ASME Journal of Fluids Engineering* 131, 091201.
- Shan, H. (2007). Numerical simulation of flow behind active vortex generators with direct forcing immersed boundary method. *International Journal of Computational Fluid Dynamics* 21(1), 49-60.
- Shan, H., L. Jiang, C. Liu, M. Love and B. Maines (2008). Numerical study of passive and active flow separation control over a NACA0012 airfoil. *Computers and Fluids* 37, 975-992.
- Singh, N. K. (2013). Prediction and Control of a Laminar Separation Bubble. PhD Thesis, Indian Institute of Technology, Kanpur, India.
- Singh, N. K. and S. Sarkar (2011). DNS of a Laminar Separation Bubble. *International Journal of Mechanical and Mechatronics Engineering* 5 (9), 1757-61.
- Smith, F. T. (1994). Theoretical prediction and design for vortex generators in turbulent boundary layers. *Journal of Fluid Mechanics* 270, 91–131.
- Sohankar, A. and L. Davidson (2003). Numerical study of heat and flow in a plate-fin heat exchanger with vortex generators. In K. Hanjalic *et al.* (Ed.). *Turbulence, Heat and Mass Transfer* 4, 1155-1162.
- Taylor, H. D. (1948a). Application of vortex generator mixing principle to diffusers.

- Research Department, United Aircraft Corporation*, Concluding Report No. R-1504-5, East Hartford, CN.
- Taylor, H. D. (1948b). Design criteria for and applications of the vortex generator mixing principle. *Research Department, United Aircraft Corporation*, Report No. M-15038-1, East Hartford, CN.
- Velte, C. M. and M. O. L. Hansen (2013). Investigation of flow behind vortex generators by stereo particle image velocimetry on a thick airfoil near stall. *Wind Energy* 16, 775-785.
- Velte, C. M., C. Braud, S. Coudert and J. M. Foucaut (2014). Vortex generator induced flow in a high Re boundary layer. *Journal of Physics*, Conference Series 555, 012102.
- Velte, C. M., M. O. L. Hansen and K. Jønck (2007). Experimental and numerical investigation of the performance of vortex generators on separation control. *Journal of Physics*, Conference Series 75, 01230.